CrossMark

ROYAL
AERONAUTICAL
SOCIETY

REGULAR PAPER

Effective aero-optical suppression by steady wall blowing and wall suction schemes for supersonic turbulent boundary layer

H. Zou , X.-L. Yang* , X.-W. Sun , W. Liu and Q. Yang

National University of Defense Technology, College of Aerospace Science and Engineering, Changsha, Hunan, Peoples Republic of China
*Corresponding author: Email: yangxl_nudt@sina.com

Abstract

As a basic flow model for engineering applications, wall-bounded turbulent flow has been widely studied in the field of aero-optics, but the flow control methods that could effectively suppress aero-optical effects are relatively rare. As an urgent requirement in engineering application, the concept of the steady wall blowing and suction is proposed by the author. Firstly, the author briefly described the flow model and physical method. Secondly, the choice of disturbance type is given. Then, the results of wall blowing-suction, suction and blowing ways based on steady and unsteady disturbance are compared. Finally, it is concluded that employing the high steady wall blowing disturbance ($A = 0.2$) could realise aero-optical suppression by around 20%. Besides, the steady wall suction scheme contributes to about 70%–80% reduction effect within a wide amplitude range ($A = 0.2$–1.0), which suppresses this effect by maintaining laminar state downstream contrasted by the baseline case.

Nomenclature

A	amplitude
C	coefficient
K_{GD}	Gladstone-Dale constant, m^3/kg
k	wave periodicity
Ma	Mach number
OPD	optical path difference
OPL	optical path length
T	temperature
t	time
b	blow
f	friction
s	suction
∞	definition text

Greek Symbol

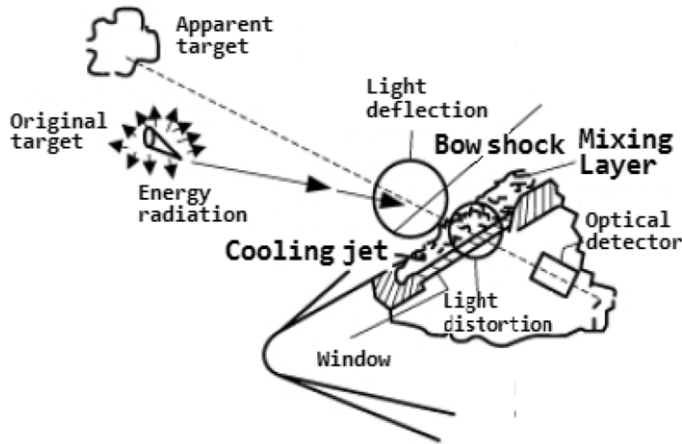|	
ρ	density
δ	boundary layer thickness

Figure 1. *Depictive picture of aero-optical effect.*

1.0 Introduction

When an imaging guidance vehicle experiences high-speed flight in atmosphere, severe distortion due to light propagation through the disturbed freestream around the optical dome would result in image aberration, jitter, intensity attenuation, and ultimately profound reduction of guidance precision (see Fig. 1). Such physical phenomenon is termed aero-optical effect. [2] The phenomenon of aero-optical effect considerably reduces the guidance precision in target-seeking application [1], so that aero-optical suppression has attached profound importance for higher resolution effectiveness [2, 3]. Relevant concepts and definitions of aero-optical parameters, such as optical path length (*OPL*) and optical path difference (*OPD*), could be referred in Ref. 4. Investigations on turbulent boundary layer [5, 6], serving as the research foundation for more complicated flow configurations, possess both great academic and engineering value in aero-optical community [7, 8].

There are many methods to suppress the aero-optical effects. As for outline design and optimisation, considering that the turbulent trasition point is closely related to the pressure gradient, changing the wall shape could keep the boundary layer more stable. Besides, we can also take proper positive schemes to control the turbulent flow, and maintain the laminar flow near the observation window to suppress this effect. Moreover, it's possible to compensate and correct the image distrotion after the mixing layer to improve image quality [3]. In previous aero-optical numerical simulations, the authors addressed the issue of fidelity by validation and verification procedures in turbulent wall-bounded flow [9], followed by the research progress of aero-optical control from both theoretical perspectives and practical attempts [10], while effective mitigation methods are rarely reported. For $M_\infty = 2.9$ supersonic turbulent boundary layer, on one hand, wall cooling does contribute to aero-optical suppression, but only a low decline rate around 19% is witnessed when the wall temperature reduces from $426.26K$ towards $241.50K$, which is additionally consolidated by Sutton statistical theory introducing Extended Strong Reynolds Analogy (ESRA) [10]. And what enhances the practical difficulty is that the cooling section should cover the turbulent flowfield as a premise. As suggested in Ref. 11, the unit Reynolds number is the main parameter to determine the transition of the ultra-high-speed boundary layer, and the wall cooling destabilises the laminar boundary layer and leads to a reduction in the transition Reynolds number. On the other hand, a proper wall suction disturbance, with its amplitude only refined in a narrow range to modify the whole region into laminar state, could realise aero-optical mitigation, and a sufficiently high suction intensity is also promising in relieving turbulence-induced aero-optical effect, while its low efficiency might limit it from practice as concluded in Ref. 10. As it stated in Ref. 12, aerodynamic performance can be improved by steady blowing active flow control. Using oblique blowing airflow, longitudinal vortices can be generated in the boundary layer. And the longitudinal vortices can provide convective redistribution of momentum in the boundary layer. This way could effectively reduce the aero-optical effect.

Other passive concepts such as the transverse spoiler rod [13] and large-eddy break-up tool [14] face considerable challenge in supersonic flow due to the possible shock wave from the interaction between the devices and thin boundary layer. As suggested in Ref. 10, investigation in this field might concentrate on higher effectiveness with simpler control effort.

From the perspective of flow mechanism, cooling the surface suppresses aero-optical effect by reducing the density fluctuation inside the turbulent boundary layer, while it is ineffective for other flow control schemes simply adjusting the transition position by wall blowing and suction or other passive strategies. To illustrate such phenomenon, despite the fact that some parameters in equations derivate from Sutton statistical theory [6, 15] are still waiting for further calibration, the turbulence-aberrated aero-optical behaviour is closely related with the local boundary thickness δ and skin friction C_f as follows

$$OPD_{rms} \propto \delta \sqrt{C_f} \tag{1}$$

The skin friction coefficient is proportionate to the velocity gradient $\partial U/\partial y$ regarding freestream stagnation from the boundary layer edge towards the non-slip surface, and the value is usually higher for the thinner boundary. The inherently negative relationship between these two parameters is why simply controlling the transition position fails to realise effective aero-optical reduction.

As suggested in Ref. 16, due to the amplification of instabilities, there are three sources of instabilities: Tollmien–Schlichting instabilities (*TSI*), cross-flow instabilities (*CFI*) and attachment line instabilities (*ALI*). These instabilities can be dampened by using boundary layer suction. Since it helps to keep the velocity profile to be a stable shape and delays separation and turbulent flow. As anticipated, effective aero-optical mitigation could be attained by steady wall suction strategy. Uncertainty in the closure coefficients of a turbulence model is an important source of error in Reynolds-averaged Navier-Stokes simulations. The authors address these aspects using state-of-the-art computational techniques, and their project aims at providing space and time-accurate experimental measurements of fluid and structure for a range of aeronautical flows as concluded in Ref. 17. Employing wall blowing and suction concepts contributes to considerable flow control efficiency despite the fact that practical application still faces great challenge [18, 19]. It is witnessed formerly in the Sec. 4.4 of Ref. 10 that fully developed turbulent flows reappear downstream under intensive suction disturbance at a sufficiently high amplitude ($A > 0.175$ therein), and there emerges a question of its reason. One possible explanation comes down to the increasing disturbance induced by unsteady suction scheme, while revealed by the reinforced trend of peak density fluctuation inside the thinner turbulent boundary layers in other blowing/suction cases 10, it is considered as another one that the accumulated unsteady effect in a thinner one from distributed wavy roughness upstream promotes turbulence downstream. To probe into this problem, simulation concerning steady and unsteady wall blowing and suction schemes is implemented in the following sections.

2.0 Physical model and numerical method

The physical model and boundary conditions (see Fig. 2), stemming from Muppidi et al's [20] $M_\infty = 2.9$ case with the static temperature and corresponding Reynolds number per meter being 170K and 2.5×10^7, has been employed in former investigations [7, 9, 10] on turbulence-aberrated aero-optical effects in supersonic turbulent boundary layer.

The grid scale via convergent analysis [9] could be referred, as well as the spatial discretization based on WCNS-E-5 (the fifth-order weighted compact nonlinear scheme) and the second-order implicit dual-time-step integration methods. The compressible Navier-Stokes equations in curvilinear coordinates have been described in detail by Zhao et al. [21] Note that the convective derivatives are handled using a sixth-order central differential formula, and take $(\partial F/\partial \xi)_j$ as an example

$$\left(\frac{\partial F}{\partial \xi}\right)_j = \frac{75}{64\Delta\xi}\left(F_{j+1/2} - F_{j-1/2}\right) - \frac{25}{384\Delta\xi}\left(F_{j+3/2} - F_{j-3/2}\right) + \frac{3}{640\Delta\xi}\left(F_{j+5/2} - F_{j-5/2}\right) \tag{2}$$
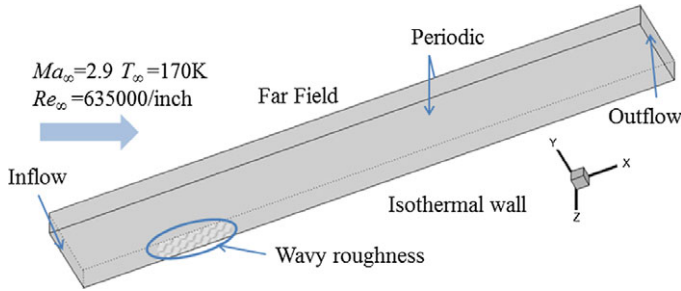
Figure 2. *Sketch of the physical problem and boundary conditions.*

where $\Delta\xi$ and $F_{j\pm1/2}$ represent the grid scale and the numerical flux at the cell edges, respectively. In this paper, Roe's difference scheme is used to solve the numerical flux

$$F_{j+1/2} = \frac{1}{2}\left[F^+\left(U_{Lj+1/2}\right) + F^-\left(U_{Rj+1/2}\right) - |A|\left(U_{Rj+1/2} - U_{Lj+1/2}\right)\right] \tag{3}$$

where $U_{Lj+1/2}$ and $U_{Rj+1/2}$ denote the quantities at the left and right cell edges, and fifth-order nonlinear weighted interpolation is implemented for efficient shock capture. The viscous terms of the governing equation are approximated using sixth-order central difference formulas with the same form as Equation (1). To obey the geometric conservation law in high-order finite difference schemes, the symmetric conservative metric method is applied for the structured grid derivatives used in coordinate transformation. Take the partial derivative of ξ_x for instance

$$\xi_x = \frac{J}{2}\left[\left(y_\eta z\right)_\zeta - \left(y_\zeta z\right)_\eta + \left(yz_\zeta\right)_\eta - \left(yz_\eta\right)_\zeta\right] \tag{4}$$

The numerical code runs in parallel to enhance the simulation efficiency. In detail, the whole computational regon is split into sub-areas through domain decomposition, and each area is distributed to a concurrent process. Communication between adjacent subdomains uses the Message Passing Interface (MPI), a standard and portable message-passing system. The simulation type is MPI distributed memory parallel, specifically the Inter MPI 2019 compiler and run time library by Tianhe-2A Supercomputer.

Quite different from other LES methods with explicit subgrid models, the effect of small-scale vortices, which are assumed to be captured artificially, is reflected on the inherent dissipation characteristics by the coarse grid system. This also prevents interference factors being induced from human knowledge when determining the empirical parameters of the subgrid model.

With regards to the computational information illustrated in Ref. 9, the unit is defaultly set as inch in the following discussion. It deserves noticing that the spanwise domain and wave periodicity k_z (see Grid 1–Grid 3 in Table 1) are both halved in order for acceptable calculation amount as issued in Ref. 9. After convergence analysis, the Grid 2 is suggested by accounting the computational expenditure since the agreement of both time-averaged velocity profiles and Reynolds stress distributions between the finer grids is reliable, and the period of two flow times is sufficient with satisfactory accuracy of error around 1% for turbulence-induced aero-optical statistic.

In previous simulation on aero-optical control by wall blowing and suction schemes in Ref. 10, with the light pupil covering the original turbulent section of $x \in [8.5, 9.9]$ where the thickness grows almost linearly from 0.075 to 0.09 in the default baseline case, the momentum excitation version by following function is exerted in laminar region of $x \in [5.5, 6.0]$ in a rectangular shape.

$$\rho v_{bs} = Au_\infty \rho_\infty f(x)\, g(z)\, h(t) \tag{5}$$

where A represents the non-dimensional disturbance amplitude, $f(x)$ and $g(z)$ are spatial function in streamwise and spanwise directions respectively, and $h(t)$ is the unsteady time term from Ref. 4

$$f(x) = 4sin\left(\theta\left[1 - cos\left(\theta\right)\right]\right) / \left(27\right)^{1/2} \tag{6}$$

Table 1. *Grid system information*

		Roughness	Grid scale	
	Computational domain	$k_x \times k_z$	$N_x \times N_y \times N_z$	$\Delta x^+ \times \Delta y^w \times \Delta z^+$
Muppidi	[4,10][0,0.5][0,0.175]	5×2	$2,401 \times 78 \times 192$	$15 \times 0.3 \times 5.4$
Grid 1	[4, 10][0, 0.5][0, 0.0875]	5×1	$1,921 \times 81 \times 65$	$18.75 \times 0.297 \times 8.28$
Grid 2			$2,401 \times 101 \times 81$	$15 \times 0.238 \times 6.625$
Grid 3			$3,001 \times 121 \times 101$	$12 \times 0.2 \times 5.3$

$$\theta = 2\pi \ (x - x_1) \ / \ (x_2 - x_1) \tag{7}$$

$$g(z) = \sum_{l=0}^{l_{max}} Z_l sin \left[2\pi l \ (z/z_{max} + \phi_l) \right] \tag{8}$$

$$\sum_{l=0}^{l_{max}} Z_l = 1 \ Z_l = 1.25 Z_{l+1} \tag{9}$$

$$h(t) = \sum_{m-1}^{m_{max}} T_m sin \left[2\pi m \ (\beta t + \phi_m) \right] \tag{10}$$

$$\sum_{m-1}^{m_{max}} T_m = 1 \ T_m = 1.25 T_{m+1} \tag{11}$$

Herein, ϕ_l and ϕ_m are random phases, and the definitions of remaining parameters could be obtained in Ref. 10. To ensure the comparability between steady and unsteady schemes, another two problems concerning the blowing and suction functions might be issued in detail, namely the disturbance type (the momentum or velocity version) and the way to realise steady and unsteady schemes.

In Equation (5), the prescribed amplitude A fails to independently decide the disturbance intensity due to the local density ρ involved, so that the velocity version by Pirozzoli et al. [19] is considered instead

$$v_{bs} = Au_\infty f(x) \ g(z) \ h(t) \tag{12}$$

In the second problem, the time term $h(t)$ should be obviously kept as constant in steady scheme, while this value, tested as 0.245 currently, could ensure the similar time-averaged amplitude compared with original unsteady one. In addition, the random phase ϕ_l of $g(z)$ in Equation (8) in each location point should be fixed after initialisation in case of erroneous unsteady effect introduced by time iteration update. Based on above discussion, the blowing v_b and suction v_s schemes could be correspondingly expressed as follows, where they are doubled after taking absolute values to keep the amplitude at A.

$$v_b = abs \left[2Au_\infty f(x) \ g(z) \ h(t) \right] \tag{13}$$

$$v_s = -abs \left[2Au_\infty f(x) \ g(z) \ h(t) \right] \tag{14}$$

The period of two flow times is employed for time-average or fluctuation statistics, which is also sufficient with satisfactory accuracy for turbulence-induced aero-optical calculation [9].

3.0 Case set and result analysis

3.1 Computing foundation for research

Apart from the baseline case, several groups comparing steady and unsteady schemes are studied in current section as listed in the first four columns in Table 2, where suffixes 'un' and 'st' denote 'unsteady' and 'steady' respectively. Only both weak and intensive conditions are issued, while the cases with

Table 2. *Case investigation and aero-optical results*

No	Concerned problem category	A	Case name	$OPD_{rms} \times 10^7$/m	Relative difference	Aero-optical change rate
0	Baseline	0	Baseline	4.029	–	–
1-un	Wall blowing	0.01	wbs_a001_un	5.205	4.77%	29.2%
1-st	and suction		wbs_a001_st	4.956		23.0%
2-un	disturbance	0.02	wbs_a02_un	5.036	2.24%	25.0%
2-st			wbs_a02_st	4.922		22.2%
3-un		0.05	wb_005_un	6.186	21.57%	53.5%
3-st	Wall blowing		wb_005_st	4.852		20.4%
4-un	disturbance	0.15	wb_015_un	6.132	47.24%	52.2%
4-st			wb_015_st	3.235		−19.7%
5-un		0.1	ws_01_un	4.750	14.20%	17.9%
5-st			ws_01_st	4.076		1.2%
6-un	Wall suction	0.2	ws_02_un	0.731	−2.41%	−81.9%
6-st	disturbance		ws_02_st	0.749		−81.4%
7-un		1.0	ws_10_un	4.784	74.67%	18.7%
7-st			ws_10_st	1.212		−69.9%

the suction amplitude being 0.2 are additionally investigated since thorough laminar state occurs in downstream plate, as a typical flow condition in former unsteady suction cases 10 for the unsteady one. In the last two columns, the 'relative difference' denotes the reduction rate of steady scheme compared with the unsteady one, and the 'aero-optical change rate' reflects the relative change between respecive case and the baseline where a negative value correpsonds to reduction effect.

It is essential to address the comparability, videlicet their time-averaged disturbance intensities, between the steady and unsteady schemes. As the wall-normal velocity plotted in Fig. 3, almost over-lapped distributions are witnessed for both blowing and suction schemes under the small amplitudes 0.05 or 0.1, consolidating the rationality of case set strategy in Section 2. It should be additionally noticed that time-averaged amplitudes can only attain the one-tenth of the prescribed ones despite the fact of corresponding transient peak values in desire.

3.2 Wall blowing and suction scheme

The boundary layer thickness and skin coefficient distributions of steady and unsteady blowing and suction schemes are plotted in Fig. 4, where weak disturbances contribute to visble transition lag towards $x = 8.0$, which is also witnessed in Ref. 10. Even though the most unsteady frequency is specified as the fundamental one β of the disturbance in Equation (10), the phase difference between the unstable wave from the wall blowing and suction disturbance and the one generated by wavy roughness is not elaborately concerned, so that the additional disturbance might not advance the transition onset position by strengthening the unstable wave as originally anticipated. This phenomenon, widely occurring in current and former investigations [10], should be further addressed by intrinsic mechanism analysis. Further increasing the unsteady disturbance amplitude obviously puts forward the transition point by the case 'wbs_a02_un', while little impact is exerted towards the boundary layer evolution concerning the steady one.

As the time-averaged OPD_{rms} values recorded in the last columns in Table 2 reveal, the steady wall blowing and suction scheme only slightly improves the imaging quality compared with the unsteady one, while aero-optical suppression in terms of the baseline case is unattainable.
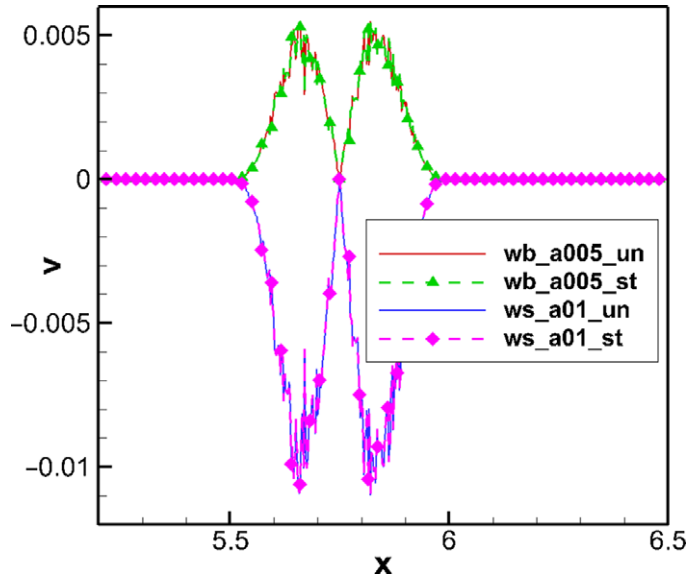
Figure 3. *Comparative distributions of time-averaged wall-normal velocity component by blowing or suction schemes.*
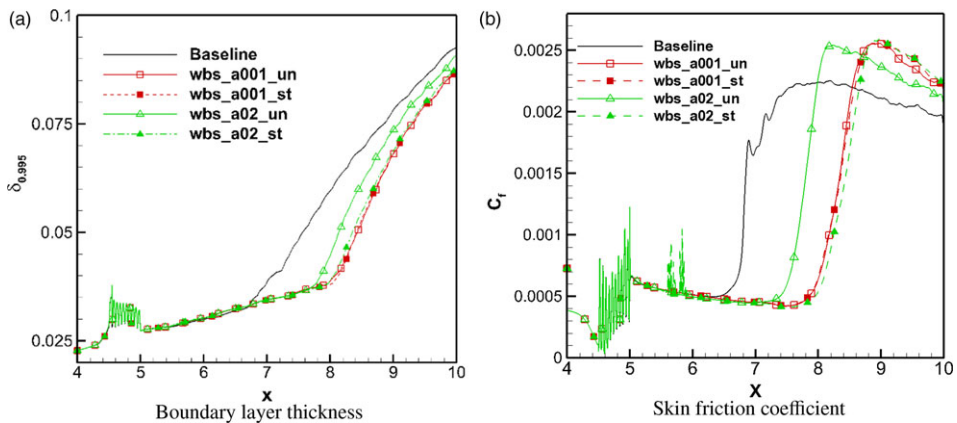

Figure 4. *Comparison of boundary layer thickness and skin friction coefficient by steady and unsteady wall blowing and suction schemes.*

3.3 Wall blowing scheme

In weak wall blowing cases 'wb_a005_un' and 'wb_a005_st', spatial transition lag occurs in Fig. 5, especially the latter one which implies the effect of steady disturbance. For the unsteady scheme, improving the blowing intensity to $A = 0.15$ simply strengthens the unsteadiness of the flowfield, thickening the boundary layer and advancing the transition position, as shown in the density contour of Fig. 6(a). It could be explained by coherent structure. In turbulent boundary layer control, coherent structure theory explains that coherent structure, which is the large scale motion that presents regularity in the turbulent boundary layer, plays an important role in momentum and energy exchange. By analysing the results of previous studies [22, 23], it could be found that: wall blowing scheme can lift the vortex structure near the wall, thus reducing the skin friction, but it would cause an increase in turbulence in the buffer zone, which in turn leads to increased friction downstream.
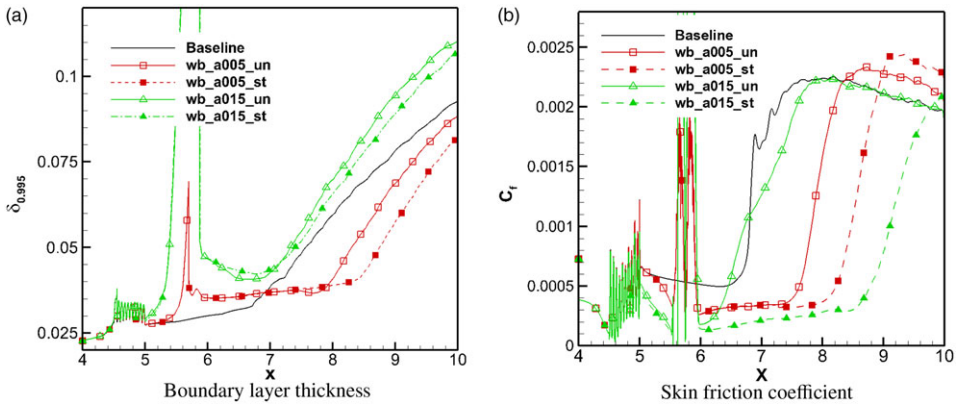
Figure 5. *Comparison of boundary layer thickness and skin friction coefficient by steady and unsteady wall blowing schemes.*
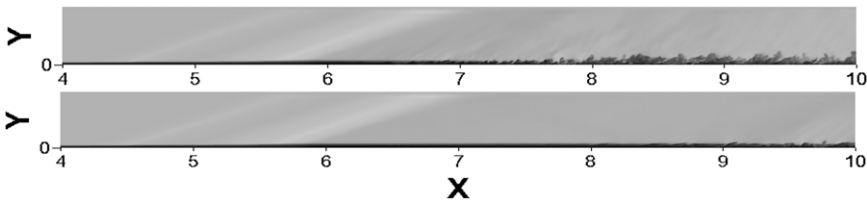

Figure 6. *Comparison of transient grey-scale density distribution in spanwise symmetric plane for intensive wall blowing cases A = 0.15 for unsteady and steady one.*

Concerning the steady one, however, a higher blowing amplitude does lead to thicker boundary layer (see Fig. 5(a)), while the transition occurs much more downstream as the friction plot evidenced in Fig. 5(b), which is additionally proved by Fig. 6(b) where most flow region tends to be laminar. And the supposition posed in section 1 coulid be confirmed; the accumulated unsteady effect in a thinner boundary layer from distributed wavy roughness upstream promotes turbulence downstream. Hence, steady disturbance does contribute to delaying transition and suppressing aero-optical effect.

In further discussion on aero-optical effect in Table 2, however, both weak and intensive steady blowing attempts present lower OPD_{rms} values than the unsteady ones, and the case 'wb_015_st' realises aero-optical reduction compared with the baseline value. It could be further anticipated that the higher the steady amplitude, the better the aero-optical mitigation effect.

3.4 Wall suction scheme

Similarly like the blowing cases, spatial transition lags more downstream for steady suction scheme than the unsteady one at a small amplitude $A = 0.1$ (see Fig. 7(a)), and their peak skin friction values are almost the same in Fig. 7(b). Further increasing the amplitude to 0.2, the boundary layers of both steady and unsteady cases show laminar state with nearly the same thickness and skin friction plots, indicating that the laminar development stage is attainable at a suitable suction intensity regardless of the disturbance type. It could be considered that wall suction scheme can capture the vortex structure near the wall, thus increasing the skin friction, but it will cause a reduction in turbulence in the buffer zone, which in turn leads to decreased friction downstream. Besides, wall suction scheme could make a thinner boundary layer and suppress aero-optical effect correspondingly. The flow states, however, thoroughly differ when $A = 1.0$ where the fully turbulent structures reappear downstream for the traditional unsteady suction, while the laminar state is maintained as additionally proved by the density contours in Fig. 8. However, as the disturbance amplitude increases too much, the OPD_{rms} value would tend to go
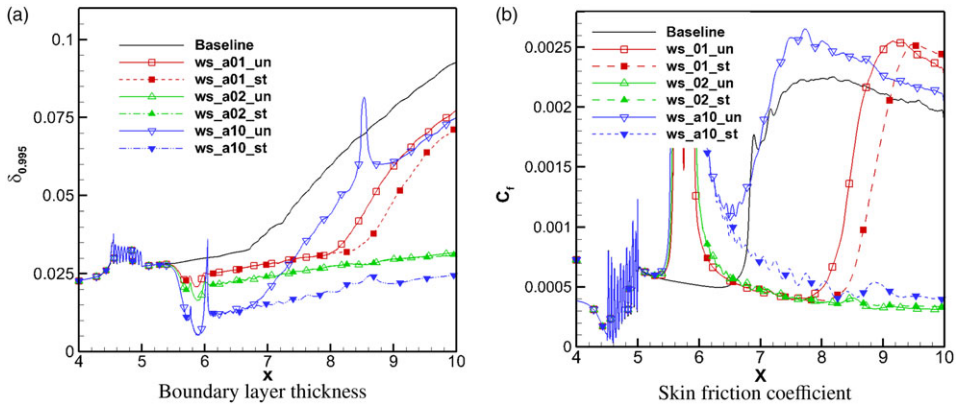
Figure 7. *Comparison of boundary layer thickness and skin friction coefficient by steady and unsteady wall suction schemes.*
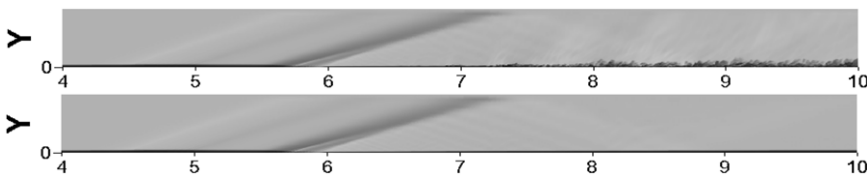

Figure 8. *Comparison of transient grey-scale density distribution in spanwise symmetric plane for intensive wall suction cases $A = 1.0$ for unsteady and steady one.*

up. But the concrete principle about the interaction between steady wall blowing/suction methods and the disturbance amplitude, and how the interaction influences the OPD_{rms} value are still unclear. This phenomenon needs further discussion.

Except for the closely presented aero-optical responses (in Table 2) for the middle suction cases providing both laminar flows, the steady strategy shows better reduction effect than the unsteady one. It is worth mentioning that exerting steady wall suction could contribute to aero-optical reduction by modifying downstream turbulence into laminar state within a wide amplitude range.

It deserves further discussion that the time-averaged OPD_{rms} of the case 'ws_a10_st' exceeds that of 'ws_a02_st', which conforms to the increasing peak density fluctuation revealed in Fig. 9. In steady suction cases, a higher intensity does lead to thinner boundary layer, while the wall-normal ρ_{rms} maximum slightly climbs up inside it for a fixed streamwise position, which implies the existence of minimum aero-optical response for steady suction schemes. Additionally, the distinguishable local maximum for the plot 'ws_a10_un' is also witnessed in Ref. 10 and has been discussed in its Sec. 4.5.

4.0 Conclusion

As urgently required in precision guidance application, the steady wall blowing and suction concept is leveraged for effective aero-optical reduction, and its advantage over the traditional unsteady one is witnessed in Fig. 8 and the last column in Table 2 due to the suppressed flow disturbance. And employing the high steady wall blowing disturbance ($A = 0.2$) could realise aero-optical suppression by around 20%, while the steady suction scheme contributes to about 70%–80% reduction effect within a wide amplitude range ($A = 0.2$–1.0) by maintaining laminar states downstream contrasted by the baseline case. The author quantitatively verified the schemes of steady wall blowing and suction with proper disturbance amplitudes, which could effectively reduce the OPD_{rms} value remarkably suppress aero-optical effect. And this investigation possesses reference value for aero-optical suppression in precision guidance in
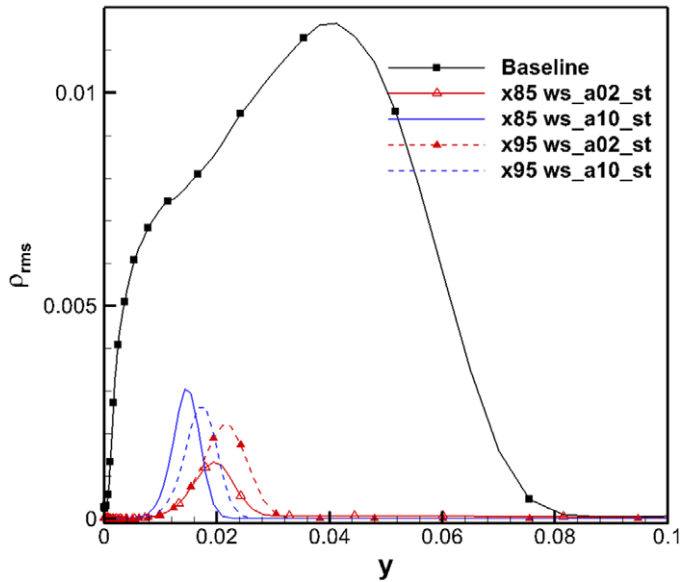
Figure 9. *Comparison of wall-normal density fluctuation distributions inside the aperture of steady suction schemes.*
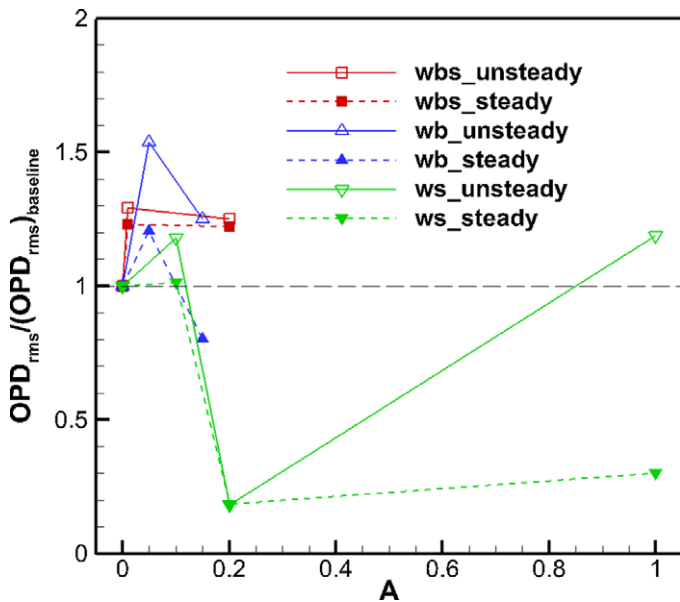

Figure 10. *Comparison of normalised time-averaged aero-optical effect by steady and unsteady disturbance for three schemes.*

engineering practice. However, once the disturbance amplitudes are too high, OPD_{rms} value would increase even using the steady disturbance. The mechanism about the concrete relationship between steady schemes and disturbance amplitudes, we can't explain clear with current work. And it needs to be discussed further.

References

[1] Jumper, E.J. and Gordeyev, S. Physics and measurement of aero-optical effects: Past and present, *Ann Rev Fluid Mech*, 2017, **49**, (1), pp 419–441.

[2] Sun, X.W., Liu, W. and Chai, Z.X. Method of investigation for numerical simulation on aero-optical effect based on WCNS-E-5, *AIAA J*, 2019, **57**, (5) pp 2017–2029.

[3] Sun, X.W. and Liu, W. Research progress of aero-optical effect (in Chinese), *Adv Mech*, 2020, **50**, p 202008.

[4] Sun, X.W., Yang, X.L. and Liu, W. Numerical investigation on aero-optical reduction for supersonic turbulent mixing layer, *Int J Aeronaut Space Sci*, 2020, **22**, pp 239–254.

[5] Sun, X.W., Yang, X.L. and Liu, W. Aero-optical and aero-heating effects of supersonic turbulent boundary layer with a tangential wall-injection film, *Phys Fluids*, 2021, **33**, p 035118.

[6] Wyckham, C.M. and Smits, A.J. Aero-optic distortion in transonic and hypersonic turbulent boundary layers, *AIAA J*, 2009, **47**, (9), pp 2159–2168.

[7] Sun, X.W. and Liu, W. Validation case for supersonic boundary layer and turbulent aero-optical investigation in high-Reynolds-number freestream by WCNS-E-5, *Proc Inst Mech Eng G J Aerosp Eng*, 2020, **234**, (15), pp 2153–2166.

[8] Ding, H.L., Yi, S.H., Zhao, X.H. and Ou Yang, T.C. Experimental investigation on aero-optical mitigation of hypersonic optical dome using microvortex generators, *AIAA J.*, 2019, **57**, (6), pp 2653–2658.

[9] Sun, X.W., Yang, X.L. and Liu, W. Validation method of aero-optical effect simulation for supersonic turbulent boundary layer, *AIAA J*, 2021, **22**, (1), pp 410–416.

[10] Sun, X.W., Yang, X.L. and Liu, W. Aero-optical suppression for supersonic turbulent boundary layer, *J Turbul*, 2021, **22**, (1), pp 1–25.

[11] Radespiel, R., Burnazzi, M., Casper, M. and Scholz, P. Active flow control for high lift with steady blowing, *Aeronaut J*, January 2016, **120**, (1223), pp 171–200.

[12] He, Y. and Morgan, R.G. Transition of compressible high enthalpy boundary layer flow over a flat plate, *Aeronaut J*, February 1994, **98**, (972), pp 25–34.

[13] Sinha, N., Arunajatesan, S. and Ukeiley, L.S. Large Eddy simulation of aero-optic flowfields and flow control application, *35th AIAA Plasmadynamics and Lasers Conference*, July 2014.

[14] Smith, A.E. and Gordeyev, S. Evaluation of passive boundary layer flow control methods for aero-optic mitigation, *51st AIAA Aerospace Sciences Meeting including the New Horizons Forum and Aerospace Exposition*, 2013.

[15] Gordeyev, S. and Juliano, J.T. Optical characterization of nozzle-wall Mach-6 boundary layers, *54th AIAA Aerospace Sciences Meeting*, 2016.

[16] Mosca, V., Karpuk, S., Sudhi, A., Badrya, C. and Elham, A. Multidisciplinary design optimisation of a fully electric regional aircraft wing with active flow control technology, *Aeronaut J*, 2022, **126**, (1298), pp 1072–1089.

[17] Da Ronch, A., Panzeri, M., Drofelnik, J. and dIppolito, R. Sensitivity and calibration of turbulence model in the presence of epistemic uncertainties, *CEAS Aeronaut J*, March 2019.

[18] Sharma, S., Shadloo, M.S., Hadjadj, A. and Kloker, M.J. Control of oblique-type breakdown in a supersonic boundary layer employing streaks, *J Fluid Mech*, 2019, **873**, pp 1072–1089.

[19] Pirozzoli, S., Grasso, F. and Gatski, T.B. Direct numerical simulation and analysis of a spatially evolving supersonic turbulent boundary layer at M=2.25, *Phys Fluids*, 2004, **16**, (3), pp 530–545.

[20] Muppidi, S. and Mahesh, K. Direct numerical simulations of roughness-induced transition in supersonic boundary layers, *J Fluid Mech*, 2012, **693**, (2), pp 28–56.

[21] Zhao, Y., Liu, W., Xu, D., Yi, S. and Elham, A. A combined experimental and numerical investigation of roughness induced supersonic boundary layer transition, *Acta Astronaut*, 2016, **118**, pp 199–209.

[22] Liepmann, H.W. The rise and fall of ideas in turbulence, *Amer Sci*, 1979, **67**, (2), pp 221–228.

[23] Tardu, S.F., and Doche, O. Active control of the turbulent drag by a localized periodic blowing dissymmetric in time, *Exp Fluids*, 2009, **47**, (1) pp 19–26.